Slow Coherency Identification and Power System Dynamic Model Reduction by using Orthogonal Structure of Electromechanical Eigenvectors

Tyuryukanov, I.; Popov, M.; van der Meijden, M.A.M.M.; Terzija, Vladimir

DOI
10.1109/TPWRS.2020.3009628

Publication date
2020

Document Version
Final published version

Published in
IEEE Transactions on Power Systems

Slow Coherency Identification and Power System Dynamic Model Reduction by Using Orthogonal Structure of Electromechanical Eigenvectors

Ilya Tyuryukanov, *Member, IEEE*, Marjan Popov, *Senior Member, IEEE*, Mart A. M. M. van der Meijden, *Senior Member, IEEE*, and Vladimir Terzija, *Fellow, IEEE*

***Abstract*—Identifying generator coherency with respect to slow oscillatory modes has numerous power system use cases including dynamic model reduction, dynamic security analysis, or system integrity protection schemes (e.g., power system islanding). Despite their popularity in both research and industry, classic eigenvector-based slow coherency techniques may not always return accurate results. The multiple past endeavors to improve their accuracy often lack a solid mathematical foundation. Motivated by these deficiencies, we propose an alternative consistent approach to generator slow coherency. Firstly, a new approach is introduced to accurately detect slow coherent generators by effectively minimizing generic normalized cuts. As a by-product, the new approach can also guide the choice of the number of slow coherent groups. Secondly, it is shown that the combination of the the proposed slow coherency approach and an enhanced version of the inertial generator aggregation method allows to produce accurate dynamic equivalents even if the selected number of generator groups is relatively low.**

***Index Terms*—Coherency identification, generator aggregation, dynamic model reduction, number of clusters, slow coherency.**

I. Introduction

COHERENCY-BASED partitioning of electric power systems has been used in many applications since its inception in 1970s [1], [2]. Initially, coherency-based generator grouping and aggregation were used to accelerate transient stability simulations of a *study area* in a bulk power grid by replacing the areas external to it with reduced-order dynamic equivalents. Besides their direct use in multiple applications involving a study area of interest, coherency-based reduced dynamic models are essential for online dynamic security assessment (DSA) [3] and DSA-related preventive or remedial control actions. Another use case of coherency-based reduced models is motivated by the aversion of system operators to share the full models of their control areas with third parties for confidentiality reasons. Besides applications to power system model reduction, coherency identification techniques are instrumental for the design of certain system integrity protection schemes (SIPS) such as intentional controlled islanding (ICI) [4]–[6], as well as the design of wide-area monitoring and control systems (WAMCS) [7], [8].

Existing power system coherency identification techniques can be broadly divided into model-based and signal-based approaches. The signal-based approaches aim to estimate coherent power system areas by analyzing the dynamic wide-area response signals, and their growing development is largely motivated by the wide availability of Synchronized Measurement Technology (SMT) [9]. The advantages of signal-based coherency approaches include high adaptation to the current operating condition and low dependence on system model data. However, the wide-area dynamic response signals are disturbance-dependent, and their processing poses several challenges including unreliable results during changing system conditions [10], sensitivity to spurious signal components [11], inconclusive signal similarities and data window lengths [10], clustering issues (e.g., choice of the number of groups) etc.

Coincidentally, model-based coherency approaches retain their significance for a number of practical applications. In particular, coherency-based model reduction is popular among practitioners, and there exist automated software tools to produce reduced dynamic equivalents from the power system model data (e.g., the DYNRED package [3], [12]). Coherency-based power system model reduction proceeds in the following three basic steps [3]. First, coherent generator groups are identified in a power network. Next, each coherent generator group outside of the study area of interest is aggregated to an equivalent generator, while the coherent generator groups inside of the study area remain unreduced. In the final step, the load buses outside of the study area are reduced by using the specialized techniques (e.g., those based on Ward reduction [13]). As each coherent group is replaced by a standard generator model, coherency-based dynamic reduction methods can be easily integrated with commercial dynamic simulation packages. This is different

Manuscript received March 4, 2020; revised June 18, 2020; accepted July 4, 2020. Date of publication July 15, 2020; date of current version February 19, 2021. This work was supported in part by the frame of the NWO's ESI-BIDA program, project ReSident (No. 647.003.004), in part by the Dutch Scientific Council NWO, in part by the consortium consisting of TSO TenneT and DSOs Alliander-Qirion, Stedin, Enduris, and in part by General Electric and VSL. Paper no. TPWRS-00346-2020. *(Corresponding author: Ilya Tyuryukanov.)*

Ilya Tyuryukanov and Marjan Popov are with the Delft University of Technology, 2628CD Delft, The Netherlands (e-mail: i.tyuryukanov@tudelft.nl; m.popov@tudelft.nl).

Mart A. M. M. van der Meijden is with the TenneT TSO B.V., 6812AR Arnhem, The Netherlands, and also with the Delft University of Technology, 2628CD Delft, The Netherlands (e-mail: mart.vander.meijden@tennet.eu).

Vladimir Terzija is with the School of Electrical and Electronic Engineering, The University of Manchester, Manchester M13 9PL, U.K. (e-mail: terzija@ieee.org).

Color versions of one or more of the figures in this article are available online at https://ieeexplore.ieee.org.

Digital Object Identifier 10.1109/TPWRS.2020.3009628

to the alternative class of reduction methods stemming from control theory [14], [15], which do not depend on the coherency information, but can only produce equivalents in the form of linear time-invariant (LTI) systems.

The classic model-based coherency techniques utilize the rotor angle mode shapes of slow system modes to detect the groups of *slow coherent* generators. Generator grouping based on slow coherency results in clustering together strongly connected generators [16]. As strong connections within an operating region is a system property, areas obtained based on slow coherency are robust and change little with varying system parameters and operating conditions. The comprehensive theory underlying slow coherency based grouping and model reduction was developed during the 1980 s and 1990s [17], [18]. Since then, some new ideas and algorithms that could contribute to the topic have emerged in various disciplines [19], [20]. This paper explores the practical implications of the close relationship between slow coherency and normalized graph cuts (Ncuts). Namely, considering slow coherency as an Ncut problem allows to consistently achieve more accurate generator groupings than with the conventional approaches. The main obstacle lies in the NP-completeness of the Ncut problem and the large solution space of its exact formulations (e.g., see [21]), which prompts the development of alternative solution methods that are able to achieve a near-global Ncut optimum in polynomial time. To resolve this issue, we propose a novel slow coherency grouping algorithm that organically integrates the new advances in spectral clustering and the classic coherency works, while revealing the favorable numbers of groups present in the system. Our findings show that Ncut values close to the global minimum are crucial for the high fidelity of slow coherency groupings. Because of this, some elements of our previously published highly efficient Ncut minimization approach [22] are adapted from minimizing standard Ncuts in sparse graphs to minimizing *generic* Ncuts in complete graphs that are related to slow coherency. Besides the precise slow coherency grouping, we propose an improvement to the *inertial aggregation* algorithm (see Section VI-A) to reduce its so-called *stiffening effect* [18], which also helps to further check the validity of coherency groupings through nonlinear dynamic reduction case studies.

From the high-level perspective, the paper has two interrelated motivations. Firstly, it shows that the popular spectral clustering method can be more that an ordinary analytics tool for power system data. By the virtue of Ncut minimization from which it derives, spectral clustering is capable of remarkably revealing the inherent structure of various power system models, some of which possess the graph Laplacian structure (e.g., branch admittance matrix, parts of power flow Jacobian [23], electromechanical power system model [3]). Secondly, the paper demonstrates that the grouping accuracy can be of crucial importance. In fact, the classic slow coherency algorithm [17] has been removed from the latest versions of the DYNRED software due to its inferior performance [12]. The new slow coherency grouping algorithm proposed in this paper uses the same model and eigenvector-based principle as the classic one, yet it allows to obtain high quality reduced dynamic models (see Section VI), thus showing that classic slow coherency can be used for dynamic model reduction despite being previously discarded for this purpose.

II. Slow Coherency

A. Basic Slow Coherency Model

The second-order electromechanical model with neglected damping is widely used to study slow coherency in power systems. It is given below in its typical compact form:

$$\boldsymbol{\Delta\ddot{\delta}} = \mathbf{M}^{-1}\mathbf{K}\boldsymbol{\Delta\delta} \tag{1}$$

where $\boldsymbol{\Delta\delta}$ is a vector of small deviations in machine rotor angles, $\mathbf{M} = \frac{2}{\omega_0}\mathbf{H}$ is a diagonal matrix of scaled machine inertias M_i, $\mathbf{H}$ is the diagonal matrix of machine inertias H_i, $i = 1, \ldots, m$, ω_0 is the nominal system frequency in rad/s, and $\mathbf{K}$ is the full matrix of synchronizing torque coefficients between the machines that is defined element-wise as follows:

$$K_{ij} = E_i^{'}E_j^{'}B_{ij}\cos(\delta_{i,0} - \delta_{j,0}) - E_i^{'}E_j^{'}G_{ij}\sin(\delta_{i,0} - \delta_{j,0}) = K_{ij}^{B} - K_{ij}^{G}, j \neq i \tag{2a}$$

$$K_{ii} = -\sum_{j=1, j\neq i}^{m} K_{ij} \tag{2b}$$

where m is the number of synchronous machines, $E_i^{'}$ is the per unit magnitude of the transient emf phasor $\underline{E_i^{'}}$ of machine i, G_{ij} and B_{ij} are the (p.u.) real and imaginary components of the (i, j) entry of the system admittance matrix reduced with respect to machines' internal nodes by using Kron reduction [24], and $\delta_{i,0}$ is the angle of $\underline{E_i^{'}}$ at the current steady-state.

The model in (1) originates from a linearized system of swing equations [24]. For high-voltage transmission power networks, the components of K_{ij} associated with the transfer conductances G_{ij} (i.e., K_{ij}^{G}) are normally much smaller than the components associated with the transfer susceptances B_{ij} (i.e., K_{ij}^{B}). If the terms K_{ij}^{G} in (2a) are neglected, the matrix $\mathbf{K}$ becomes symmetric for transmission networks without phase shifters, and it is further referred to as $\mathbf{K^B}$. The matrix $\mathbf{K^B}$ is often used in power system literature instead of the matrix $\mathbf{K}$, as its symmetry and negative semidefiniteness are favorable analytic properties [4].

B. Slow Coherency and Power System Oscillations

The eigenvalues $\lambda_1, \ldots, \lambda_m$ of the matrix $\mathbf{M}^{-1}\mathbf{K}$ closely match with the squared frequencies of the electromechanical system modes, and the corresponding eigenvectors closely match with the rotor angle shapes of these modes [3]. A rotor angle mode shape describes the rotor angle oscillation pattern at the specific modal frequency [25]. That is, entries i and j of an eigenvector $\boldsymbol{V}_l$ having the same sign and a similar magnitude indicate the near-coherency of rotor angles δ_i and δ_j at the frequency $\sqrt{|\lambda_l|}$. However, electromechanical oscillations usually involve multiple frequency components, which motivates analyzing coherency for multiple mode shapes.

By its definition, slow coherency describes the coherency of rotor swings with respect to the slowest system modes [3]. Given

the k slowest eigenvectors of $\mathbf{M}^{-1}\mathbf{K}$ combined into the matrix $\mathbf{V} = [\boldsymbol{V}_1, \ldots, \boldsymbol{V}_k]$, the coherency of rotor angles δ_i and δ_j for the frequencies $\sqrt{|\lambda_1|}, \ldots, \sqrt{|\lambda_k|}$ can be characterized by the similarity of rows i and j of $\mathbf{V}$, which is analogous to the aforementioned rotor angle mode shape analysis. Noteworthy, the slowest eigenvector $\boldsymbol{V}_1$ corresponding to $\lambda_1 = 0$ has all its entries equal to the same value. This so-called *DC mode* seemingly contains no information about the relative rotor swings. However, its importance for slow coherency identification is justified both from the perspective of classic slow coherency theory (see [17, Chapter 5]) and the Ncut perspective of this paper.

Slow coherency is traditionally associated with inter-area oscillations. In large-scale power systems, it is common to have generation and load areas to be interconnected by long transmission lines. Such an area-based structure manifests itself in the eigenvalues of $\mathbf{M}^{-1}\mathbf{K}$ being separated into slow and fast modes. This relationship between the time-scale separation and the strength of inter-area connections is a fundamental property that is also related to the notions of decomposability, localizability, and state aggregation (see [16], [17]).

C. Analogy Between Slow Coherency and Normalized Cuts

By inspecting the structure of the matrix $\mathbf{K^B}$ introduced in Section II-A, it can be noted that $\mathbf{K^B}$ corresponds to a negated graph Laplacian matrix (e.g., see [4]). This fact serves as the main theoretical basis of our proposed slow coherency framework, which warrants considering it in more detail while also introducing the important definitions and notation.

If $\mathbf{K^B}$ is seen as a graph Laplacian matrix, it is possible to introduce an *electromechanical graph* $\mathscr{G} = (\mathcal{V}, \mathcal{E}, w, \mu)$ based on $\mathbf{K^B}$ and $\mathbf{M}$ [4]. The node set $\mathcal{V} = \{1, \ldots, m\}$ corresponds to all synchronous machines, and the edge set $\mathcal{E} = \{(i,j) \,|\, i,j \in \mathcal{V}, i \neq j\}$ defines a complete graph. The edge weights are induced by $\mathbf{K^B}$ as $w(i,j) = K^B_{ij}, \forall (i,j) \in \mathcal{E}$, and the node weights $\mu(i) = M_i, \forall i \in \mathcal{V}$. For $\mathscr{G}$, the generic Ncut minimization problem, which plays the key role in the slow coherency grouping process, is stated as:

$$\text{minimize} \quad \text{Ncut}_M(\widetilde{\mathbf{X}}) = \frac{1}{k}\sum_{j=1}^{k} \frac{\widetilde{\boldsymbol{X}}_j^T(-\mathbf{K^B})\widetilde{\boldsymbol{X}}_j}{\widetilde{\boldsymbol{X}}_j^T\mathbf{M}\widetilde{\boldsymbol{X}}_j} \tag{3a}$$

$$\text{subject to:} \quad \widetilde{\mathbf{X}} \in \{0,1\}^{m\times k}, \widetilde{\mathbf{X}}\mathbf{1}_{k\times 1} = \mathbf{1}_{m\times 1} \tag{3b}$$

where k is the number of groups and $\mathbf{1}_{m\times 1}$ is an all-ones column vector. In (3), machines' group assignment is modeled with binary *group indicator vectors*. If $\widetilde{\boldsymbol{X}}_1$ is the indicator vector of group $\mathcal{C}_1$, $\widetilde{\boldsymbol{X}}_1 = [f_1, \ldots, f_n]^T$ and $f_i = 1$ if node i belongs to $\mathcal{C}_1$ and $f_i = 0$ otherwise. For a k-way grouping, a binary *partition indicator matrix* can be defined as a concatenation of groups' indicator vectors: $\widetilde{\mathbf{X}} = [\widetilde{\boldsymbol{X}}_1, \ldots, \widetilde{\boldsymbol{X}}_k]$.

The definition in (3) differs from the classic Ncut definition by including scaled inertias as *generic graph node weights* instead of using weighted node degrees as graph node weights [19], [26]. The individual terms in (3) are given as:

$$\phi_M(\mathcal{C}) = \frac{\widetilde{\boldsymbol{X}}_{\mathcal{C}}^T(-\mathbf{K^B})\widetilde{\boldsymbol{X}}_{\mathcal{C}}}{\widetilde{\boldsymbol{X}}_{\mathcal{C}}^T\mathbf{M}\widetilde{\boldsymbol{X}}_{\mathcal{C}}} = \frac{\sum_{i\in\mathcal{C}, j\in\mathcal{V}\setminus\mathcal{C}} K^B_{ij}}{\sum_{i\in\mathcal{C}} M_i} \tag{4}$$

where $\widetilde{\boldsymbol{X}}_{\mathcal{C}} \in \{0,1\}^{m\times 1}$ is the indicator vector of the group $\mathcal{C}$. We call (4) *generic subgraph expansion* by analogy to both theoretically and practically important *expansion ratios* that form the classic NCut minimization objective [26].

The Ncut problem in (3) is an NP-complete discrete optimization problem even on planar graphs and for $k = 2$ [19]. To overcome this issue, the authors of [20] perform the change of variables in (3) by introducing a *scaled partition matrix* $\widetilde{\mathbf{Z}}$:

$$\widetilde{\mathbf{Z}} = \widetilde{\mathbf{X}}(\widetilde{\mathbf{X}}^T\mathbf{M}\widetilde{\mathbf{X}})^{-\frac{1}{2}}$$

Next, the original constraints of (3) are relaxed, which reduces problem (3) to a trace minimization problem:

$$\text{minimize} \quad \text{Ncut}^{SR}_M(\mathbf{Z}) = \frac{1}{k}\text{tr}\left(\mathbf{Z}^T\left(-\mathbf{K^B}\right)\mathbf{Z}\right) \tag{5a}$$

$$\text{subjectto:} \quad \mathbf{Z}^T\mathbf{M}\mathbf{Z} = \mathbf{I_k} \tag{5b}$$

Where $\mathbf{Z}$ is a continuous relaxation of $\widetilde{\mathbf{Z}}$ and (5b) helps to model the original cost function. The relaxed Ncut minimization problem (5) can be directly solved using the Rayleigh-Ritz theorem and its extensions [20]. Namely, the optimal objective value of (5) is given by the negated sum of the k smallest magnitude eigenvalues of $\mathbf{M}^{-1}\mathbf{K^B}$, and the optimal solution is given by the corresponding eigenvectors of $\mathbf{M}^{-1}\mathbf{K^B}$ combined into the matrix $\mathbf{Z}$. Therefore, the slow eigensubspace of $\mathbf{M}^{-1}\mathbf{K^B}$ that is used for slow coherency identification is also the optimal solution to the relaxed Ncut problem in (3).

III. Recovering the Orthogonal Structure of Electromechanical Eigenvectors

The last sentence of Section II-C explains the rationale behind using spectral clustering for the detection of slow coherent machines. However, the Ncut_M problem in (3) is different from the usual normalized spectral clustering (see [26]). In particular, the eigenvalues of $\mathbf{M}^{-1}\mathbf{K^B}$ are not restricted to $[0, -2]$, the generic expansion (4) is not bounded in [0, 1] and $\mathbf{K^B}$ represents a complete graph. Coincidentally, solution accuracy close to the global optimality is required, as wrongly grouping even a single important generator can pose a serious problem. In this section, we are introducing a crucial component of a highly accurate spectral clustering algorithm tailored to solving (3) that is further elaborated in Section IV.

From Section II-C, the slowest eigenvectors of $\mathbf{M}^{-1}\mathbf{K^B}$ represent the optimal solution to the spectral relaxation of (3). As shown in [20], this optimal solution $\mathbf{Z} = [\boldsymbol{Z_1}, \ldots, \boldsymbol{Z_k}]$ is invariant under orthogonal linear transformations. The rows of $\mathbf{Z}$ can be viewed as Euclidean point coordinates of the corresponding machines, which results in a *spectral embedding* of the graph $\mathscr{G}$ into $\mathbb{R}^k$. Orthogonal linear transformations can be used for the alignment of spectral embeddings with the canonical coordinate system of $\mathbb{R}^k$ to facilitate the group assignment process (e.g., see Fig. 1). In [22], we have proposed a robust algorithm to

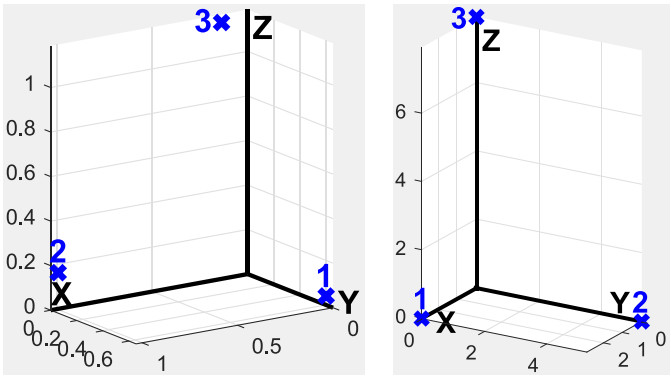

(a) Unity-length normalized (b) Mass-normalized

Fig. 1. Aligned eigenvectors of the electromechanical model of the IEEE 9 bus test system.

align *normalized spectral embeddings* with the standard basis. A normalized spectral embedding corresponds to the matrix $\mathbf{X}$ that is obtained from $\mathbf{Z}$ by normalizing the rows of $\mathbf{Z}$ to length one:

$$X_{ij} = Z_{ij} \Big/ \left(\sum_{j=1}^{k} Z_{ij}^2 \right)^{1/2} \tag{6}$$

However, the columns $\mathbf{X}$ are no longer the eigenvectors of $\mathbf{M}^{-1}\mathbf{K}^{\mathbf{B}}$ and thus no longer the proper minimizers of (5). Moreover, the information about the row magnitudes of $\mathbf{Z}$ that is lost due to (6) is significant for slow coherency identification [2]. Therefore, aligning row-normalized spectral embeddings $\mathbf{X}$ can be seen as a successful heuristic, but more precise slow coherency results can be achieved by considering both the angular and radial separation of the rows of $\mathbf{Z}$ by formulating the spectral embedding alignment problem as follows:

$$\begin{aligned} &\text{minimize} \quad J(\mathbf{R}) = \frac{1}{m} \sum_{i=1}^{m} \sum_{j=1}^{k} \frac{[\mathbf{ZR}]_{ij}^2}{U_i^2} \\ &\text{subjectto:} \quad \mathbf{R}^T\mathbf{R} = \mathbf{I_k} \end{aligned} \tag{7}$$

where $\mathbf{R} \in \mathbb{R}^{k \times k}$ is an orthogonal matrix, $U_i = \max_j [\mathbf{ZR}]_{ij}$, and $\mathbf{I_k}$ is the identity matrix of size k.

The *alignment cost* J in (7) is preferred to its counterpart from [20] because it is valid for any real matrices $\mathbf{A} \in \mathbb{R}^{m \times k}$, not only row-normalized ones. However, the optimization of (7) solely by the original approach in [27] is less scalable and more prone to local optima. The following combined approach consistently outperforms the alternatives in optimizing (7):

1) Obtain the row-normalized matrix $\mathbf{X}$ from $\mathbf{Z}$ using (6).
2) Align the normalized spectral embedding in $\mathbf{X}$ with the standard basis using the robust alignment algorithm from [22]. Store the final aligning orthogonal matrix as $\mathbf{R}^*$.
3) Use the eigenvector matrix $\mathbf{ZR}^*$ as an initialization to further minimize (7) with a gradient descent (GD) based algorithm similar to [27].

In the above procedure, step 2 significantly improves the robustness to local optima. By ignoring the row magnitudes in $\mathbf{Z}$, it identifies the major k directions in the normalized spectral k-embedding. At step 3, the rows of $\mathbf{Z}$ are transformed by $\mathbf{R}^*$ to align them with the major directions identified at step 2. As the row magnitudes are no longer ignored, an additional GD-based minimization of (7) is performed to account for them; the improvements achieved at step 3 are typically quite small.

Another important issue is the scaling of the columns of $\mathbf{Z}$. For the classic coherency grouping algorithm in [17], the eigenvector scaling issue was not elaborated. For the tolerance-based coherency algorithm [3], it was recommended to scale each electromechanical eigenvector to length one (this scaling is also implicit in many eigensolvers). The eigenvector scaling adopted in this paper hinges on constraint (5b) for valid optimal solutions of the spectral relaxation in (5). Eigenvectors satisfying (5b) are known as *mass-normalized* eigenvectors. The benefits of using mass-normalized electromechanical eigenvectors for coherency identification are illustrated on an example involving the IEEE 9 bus test system.

The electromechanical model data of the IEEE 9 bus test system can be found e.g. in [24]. This test system contains only three generators, so if three coherent groups are requested, each generator is expected to be perfectly clustered into its own group. The unit-length normalized eigenvectors $\mathbf{V}$ and mass-normalized eigenvectors $\mathbf{Z}$ of the matrix $\mathbf{M}^{-1}\mathbf{K}$ corresponding its three eigenvalues {0, -75.54, -179.15} are:

$$\mathbf{V} = \begin{bmatrix} 0.577 & 0.315 & -0.040 \\ 0.577 & -0.824 & -0.296 \\ 0.577 & -0.470 & 0.954 \end{bmatrix} \quad \mathbf{Z} = \begin{bmatrix} 2.39 & 1.594 & -0.30 \\ 2.39 & -4.172 & -2.22 \\ 2.39 & -2.381 & 7.17 \end{bmatrix}$$

The results of applying spectral embedding alignment the above two eigenvector matrices can be seen in Fig. 1. Fig. 1b shows that aligning the mass-normalized eigenvectors in $\mathbf{Z}$ produces a discrete eigenvector matrix (i.e., the expected perfect group assignment is achieved), while Fig. 1a illustrates the impossibility of achieving the same result with the unity-length normalized eigenvectors in $\mathbf{V}$. The perfect alignment of eigenvectors in $\mathbf{Z}$ is despite employing the original non-symmetric matrix $\mathbf{K}$ (see [17, Chapter 4]). Thus, the $\mathbf{M}$-orthogonality constraint (5b), which is not inherent in model (1), allows to best reveal the orthogonal structure of electromechanical eigenvectors.

IV. Slow Coherency Grouping Algorithm

A. Estimation of Group Cores

The first step of the new slow coherency grouping algorithm shares similarities with the cluster core estimation process from our previous work [22]. To avoid repetition, this section mostly focuses on the crucial differences of the *group cores* estimation process that is summarized as Algorithm 1 from the previously proposed *cluster cores* estimation process.

According to [17], it is beneficial to choose machines with *large and linearly-independent* rows in the electromechanical eigenvector matrix as reference machines of the coherent areas.

Thus, the aligned mass-normalized electromechanical eigenvectors in $\mathbf{Z}^* = \mathbf{Z}\mathbf{R}^*$ are used in Algorithm 1 to preserve the row magnitude information that is valuable for the coherency analysis. In Algorithm 1, the largest rows of $\mathbf{Z}^*$ that best indicate the reference machines of each group are always considered first. However, without row normalization, the entries magnitudes in the columns of $\mathbf{Z}^*$ may vary considerably (e.g., see Fig. 1b), which makes it difficult to set a fixed threshold up to which each column of $\mathbf{Z}^*$ can be considered independently from the others. To solve this issue, the columns of the row-normalized eigenvector matrix $\mathbf{X}^*$ (see line 4 in Algorithm 1) are used in combination with a fixed threshold value γ, and the order of entries in a column of $\mathbf{X}^*$ is determined by the descending order of magnitudes of the corresponding column of $\mathbf{Z}^*$.

Another issue arising due to possible large magnitude differences of the entries in various columns of $\mathbf{Z}^*$ is the possibility of multiple column maxima sharing the same row of $\mathbf{Z}^*$. In such cases, the same machine can be assigned to multiple groups unless some extra measures are taken. The permutation of the columns of $\mathbf{Z}^*$ at line 3 of Algorithm 1 establishes the priority order for the columns of $\mathbf{Z}^*$ so that the prospective machine groups featuring the largest entries in their respective columns are considered first. Additionally, lines 19–20 ensure that no row of $\mathbf{Z}^*$ is selected for more than one group.

For Algorithm 1, the best results are obtained with γ being set to the lowest reliable value of $\sqrt{2}/2$. As γ is directly set to $\sqrt{2}/2$, the gains achievable by the cluster core refinement described in [22] diminish. Consequently, the refinement stage is not used to simplify the algorithm. Finally, the minimum group size requirement looses its meaning (i.e., if a single large machine constitutes a group, it must be treated as such).

Algorithm 1: Estimation of Machine Group Cores.

Input: Aligned eigenvectors $\mathbf{Z}^*$, matrix $\mathbf{K^B}$, matrix $\mathbf{M}$

1: $\gamma \leftarrow \sqrt{2}/2$ ▷Eigenvector threshold γ gets the lowest value
2: Reorder the columns of $\mathbf{Z}^*$ in the descending order of the maximum absolute elements of each column.
3: $\mathbf{X}^* \leftarrow$ Normalize rows of $\mathbf{Z}^*$ using (6)
4: **for** $l = 1$ to k **do**
5: $\boldsymbol{Z} \leftarrow \mathbf{Z}^*[1, \ldots, m; l]$ ▷l^{th} column of $\mathbf{Z}^*$
6: $\boldsymbol{X} \leftarrow \mathbf{X}^*[1, \ldots, m; l]$ ▷l^{th} column of $\mathbf{X}^*$
7: $\boldsymbol{ord} \leftarrow$ Descending order of entries in $\boldsymbol{Z}$
8: $j \leftarrow 0$
9: **for** $i \leftarrow 1, \ldots, m$ **do**
10: **if** $\boldsymbol{X}[\boldsymbol{ord}[i]] > \gamma$ **then**
11: $j \leftarrow j + 1$
12: $\boldsymbol{core}[j] \leftarrow \boldsymbol{ord}[i]$
13: $\boldsymbol{phi}[j] \leftarrow \phi_M(\mathbf{K^B}, \mathbf{M}, \boldsymbol{core})$ ▷(4)
14: **end if**
15: **end for**
16: $j^* \leftarrow \text{argmin}\boldsymbol{phi}$
17: $\mathcal{C}_l \leftarrow \{\boldsymbol{core}[1, \ldots, j^*]\}$
18: $\mathbf{Z}^*[\mathcal{C}_l; 1, \ldots, k] = 0$ ▷Set elements with row indices $\mathcal{C}_l$
19: $\mathbf{X}^*[\mathcal{C}_l; 1, \ldots, k] = 0$ ▷and column indices $1, \ldots, k$
20: **end for**

Output: Machine group cores $\mathcal{C}_1, \ldots, \mathcal{C}_k$

B. Greedy Assignment of Remaining Machines

An execution of Algorithm 1 may not classify every machine to a group core. The *remaining machines* that do not belong to any group core form a set $\mathcal{R}$. These machines are similar to *loosely coherent machines* from literature [3], [17]. As the electromechanical graph $\mathscr{G}$ is a complete graph, the cluster connectivity constraint becomes automatically satisfied. To exploit this problem property, a greedy machine assignment algorithm is proposed that often exceeds the results of the min-cut recursive bisection:

1) Evaluate the generic expansions (4) of each of the machine group cores $\mathcal{C}_1, \ldots, \mathcal{C}_k$ obtained from Algorithm 1 as $\phi_M(\mathcal{C}_1), \ldots, \phi_M(\mathcal{C}_k)$.
2) Attempt to move each remaining machine $j \in \mathcal{R}$ to every group core and evaluate the signed differences in generic expansions $\Delta\phi_M(\mathcal{C}_l \cup j) = \phi_M(\mathcal{C}_l) - \phi_M(\mathcal{C}_l \cup j), l = 1, \ldots, k, j \in \mathcal{R}$ resulting from these moves.
3) Identify the largest signed difference $\Delta\phi_M(\mathcal{C}_{l*} \cup j^*)$, where $\mathcal{C}_{l*}$ and j^* are respectively the group core and the remaining machine involved in the move.
4) Perform the following updates: $\phi_M(\mathcal{C}_{l*}) \leftarrow \phi_M(\mathcal{C}_{l*} \cup j^*)$, $\mathcal{C}_{l*} \leftarrow \mathcal{C}_{l*} \cup j^*$, $\mathcal{R} \leftarrow \mathcal{R} \setminus j^*$.
5) Repeat steps 2, 3, 4 until all remaining machines are assigned to a group core (i.e., until $\mathcal{R} = \emptyset$).

In the above algorithm, the incremental updates of group cores expansions at step 2 can be implemented in a computationally efficient manner by using the following scheme:

$$d_i = \sum_{j=1}^{m} K_{ij}^B, \forall i \in \mathcal{V} \tag{8a}$$

$$\text{vol}(\mathcal{C}_l) = \sum_{i \in \mathcal{C}_l} d_i, l = 1, \ldots, k \tag{8b}$$

$$\mu(\mathcal{C}_l) = \sum_{i \in \mathcal{C}_l} M_i, l = 1, \ldots, k \tag{8c}$$

$$\text{links}(\mathcal{C}_l, \mathcal{C}_l) = \sum_{i \in \mathcal{C}_l, j \in \mathcal{C}_l} K_{ij}^B, l = 1, \ldots, k \tag{8d}$$

$$\phi_M(\mathcal{C}_l) = \frac{\text{vol}(\mathcal{C}_l) - \text{links}(\mathcal{C}_l, \mathcal{C}_l)}{\mu(\mathcal{C}_l)}, l = 1, \ldots, k \tag{8e}$$

where d_i is the *weighted degree* of node i in the graph $\mathscr{G}$, $\text{vol}(\mathcal{C}_l)$ is the *volume* of the group $\mathcal{C}_l$ [26], $\mu(\mathcal{C}_l)$ is the total node weight of the group $\mathcal{C}_l$ and $\text{links}(\mathcal{C}_l, \mathcal{C}_l)$ is the total weight of the edges inside of the group $\mathcal{C}_l$. Thus, to compute the change of $\phi_M(\mathcal{C}_l)$ due to moving a single machine to or from the group $\mathcal{C}_l$, the quantities $\text{vol}(\mathcal{C}_l)$, $\mu(\mathcal{C}_l)$ and $\text{links}(\mathcal{C}_l, \mathcal{C}_l)$ need to be updated accordingly. Updating $\text{vol}(\mathcal{C}_l)$ and $\mu(\mathcal{C}_l)$ involves a simple addition or subtraction, as the weighted degrees d_i of the nodes in $\mathscr{G}$ can be precomputed and the scaled machine inertias M_i belong to the problem data in (1). Updating $\text{links}(\mathcal{C}_l, \mathcal{C}_l)$

involves adding or subtracting the term $2\sum_{i\in\mathcal{C}_l} K_{ij}^B$, where j is the machine moved to or from $\mathcal{C}_l$. This update scheme is also used in Algorithm 1 at line 14.

C. Greedy Search Based Group Refinement

The mass-normalized electromechanical eigenvectors in $\mathbf{Z}$ represent an optimal solution to a *continuous relaxation* (5) of the NP-complete problem in (3). This implies a possibility of suboptimal groupings by Algorithm 1, especially if the alignment cost in (7) is high. Due to NP-completeness of (3), greedy machine assignments described in Section IV-B cannot be guaranteed to converge close to the global optimum of (3). Because of these complications, the solutions obtained by the methods from Sections IV-A and IV-B may noticeably benefit from graph cut refinement [28]. The following algorithm similar to the one from Section IV-B has been successfully applied to improve the Ncut_M values:

1) Evaluate the generic expansions (4) of the input machine groups $\mathcal{C}_1,\ldots,\mathcal{C}_k$ as $\phi_M(\mathcal{C}_1),\ldots,\phi_M(\mathcal{C}_k)$.
2) Attempt to move each machine $j\in\mathcal{V}$ from its own group $\mathcal{C}_f$ to every other group $\mathcal{C}_t$ unless $\mathcal{C}_f$ is a group containing a single machine. Evaluate the signed differences $\Delta\phi_M(\mathcal{C}_t\cup j)=\phi_M(\mathcal{C}_t)-\phi_M(\mathcal{C}_t\cup j)$ and $\Delta\phi_M(\mathcal{C}_f\setminus j)=\phi_M(\mathcal{C}_f)-\phi_M(\mathcal{C}_f\setminus j)$ for $j\in\mathcal{V}, (\mathcal{C}_f\ni j)\wedge(|\mathcal{C}_f|>1), \mathcal{C}_t\in\{\mathcal{C}_1,\ldots,\mathcal{C}_k\}\setminus\mathcal{C}_f$.
3) Identify the largest signed difference $\Delta\phi_M(\mathcal{C}_{t*},j^*)=\Delta\phi_M(\mathcal{C}_{t*}\cup j^*)+\Delta\phi_M(\mathcal{C}_{f*}\setminus j^*)$, where $\mathcal{C}_{t*}$ and j^* are respectively the receiving group and the machine to be moved from the sending group $\mathcal{C}_{f*}$.
4) If $\Delta\phi_M(\mathcal{C}_{t*},j^*)>0$, perform the following updates: $\phi_M(\mathcal{C}_{t*})\leftarrow\phi_M(\mathcal{C}_{t*}\cup j^*)$, $\phi_M(\mathcal{C}_{f*})\leftarrow\phi_M(\mathcal{C}_{f*}\setminus j^*)$, $\mathcal{C}_{t*}\leftarrow\mathcal{C}_{t*}\cup j^*, \mathcal{C}_{f*}\leftarrow\mathcal{C}_{f*}\setminus j^*$.
5) Repeat steps 2, 3, 4 until $\Delta\phi_M(\mathcal{C}_{t*},j^*)\le 0$.

The full potential of the proposed Ncut refinement algorithm can be realized by running it multiple times with different initial machine groupings. Diverse initial groupings lead to an increased variety of solutions of (3) at the termination of the greedy refinement process, some of which could be close or equal to the global optimum of (3). Meaningful initial machine groupings can be generated based on the output results of Algorithm 1 (i.e., the machine group cores and the set of remaining machines $\mathcal{R}$). In Section V, the initial machine groupings were obtained by running Algorithm 1 followed by the greedy assignment of the machines in $\mathcal{R}$ (see Section IV-B) and by several random group assignments of the machines in $\mathcal{R}$. For Sections V–VI, 15 random initializations were used.

D. Comparison of Machine Assignment and Node Refinement

The greedy assignment of Section IV-B and the above Ncut refinement share a lot of similarities. In the both algorithms, a machine is taken from one group and sequentially moved to all others. The major difference between the two consists in the source set from which the machines are moved. For the greedy assignment the source set is $\mathcal{R}$ and the receiving sets are $\mathcal{C}_1,\ldots,\mathcal{C}_k$. For the Ncut refinement, $\mathcal{R}$ is empty and the machines are moved between $\mathcal{C}_1,\ldots,\mathcal{C}_k$. The results of these moves are evaluated using the update scheme in (8). In Section IV-B, the best move is implemented at every step until all machines in $\mathcal{R}$ are assigned. In Section IV-C, the best moves are executed only until they improve the objective (3a).

V. Linear Model Reduction Results

A. Grouping Accuracy Evaluation

One way to access the accuracy of a slow coherency machine grouping is by comparing the slow eigenvalues of the full model (1) with the eigenvalues of an aggregate linear model based on that machine grouping. To compare the errors in slow eigenvalues resulting from machine groupings obtained from different algorithms, the linear *inertial aggregate model* described in [3], [17] is going to be used. Although the eigenvalue errors can be made smaller by using the alternative *slow coherency aggregate model*, a less successful machine grouping will still produce higher errors than a more successful one. Moreover, the inertial aggregate model has an attractive physical meaning related to the inertial generator aggregation method [18] considered in Section VI.

To evaluate the eigenvalue errors of reduced linear electromechanical models resulting from various machine groupings, the mean percentage eigenvalue error is used:

$$\overline{\delta\lambda}=\frac{1}{k}\sum_{i=1}^{k}\frac{|\lambda_{a,i}-\lambda_{f,i}|}{|\lambda_{f,i}|}\cdot 100 \tag{9}$$

where $\lambda_{f,i}$ is the i slow eigenvalue of the full electromechanical model ($\mathbf{M}^{-1}\mathbf{K}$ or $\mathbf{M}^{-1}\mathbf{K^B}$) and $\lambda_{a,i}$ is the eigenvalue of the aggregate electromechanical model closest to $\lambda_{f,i}$.

B. NPCC 48-Machine Test System

The Northeast Power Coordinating Council (NPCC) 48-machine test system contains 140 buses, 48 of which have synchronous machines. It represents the parts of the electric power grid in the Northeastern U.S. and Southeast Canada. The NPCC 48-machine test system has often been used in generator coherency studies (e.g., in [3], [18]); many of these studies also include the system's geographical diagram, while its electromechanical model data is available in PST [29].

First, the alignment cost minimization method described in Section III is applied to the first 2,...,14 mass-normalized eigenvectors of the studied test system. In Fig. 2, the cost in (7) is minimized both for the eigenvectors of $\mathbf{M}^{-1}\mathbf{K}$ (i.e., non-symmetric $\mathbf{K}$) and the eigenvectors of $\mathbf{M}^{-1}\mathbf{K^B}$. The results for $\mathbf{M}^{-1}\mathbf{K^B}$ aim to show the ideal outcome of our spectral clustering based grouping algorithm that assumes a symmetric similarity matrix. Noteworthy, one of the local minima of the curves in Fig. 2 corresponds to grouping the machines into 9 areas – the choice that was previously advocated in [3], [17]. Other minima correspond to 3 and 6 areas. Such local minima correspond to relatively cohesive and well-decoupled groupings at various degrees of granularity. The final choice of the group number depends on the actual problem requirements, as some applications benefit from a few larger groups, while others require a smaller group size.

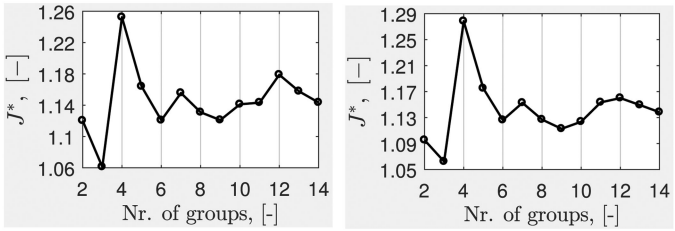

(a) Eigenvectors of $\mathbf{M}^{-1}\mathbf{K}$ (b) Eigenvectors of $\mathbf{M}^{-1}\mathbf{K^B}$

Fig. 2. Variation of alignment cost (7) for the electromechanical eigenvectors of the NPCC 48-machine test system.

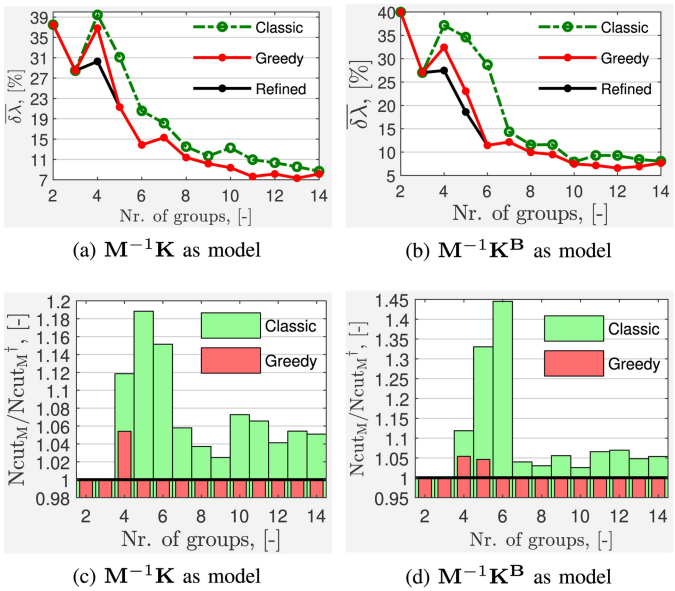

(a) $\mathbf{M}^{-1}\mathbf{K}$ as model (b) $\mathbf{M}^{-1}\mathbf{K^B}$ as model

(c) $\mathbf{M}^{-1}\mathbf{K}$ as model (d) $\mathbf{M}^{-1}\mathbf{K^B}$ as model

Fig. 3. Mean eigenvalue errors of inertial aggregate models based on groupings of the NPCC 48-machine system produced by three algorithms and associated generic Ncuts.

In any case, group numbers featuring a relatively high J-cost should be avoided.

To show the effectiveness of the approach in Section IV, its results are compared with those of the well-known slow coherency grouping algorithm [17]. These two algorithms are directly comparable, as they both return the specified number of groups k by using the k slowest electromechanical eigenvectors. The resulting mean percentage eigenvalue errors (9) are shown in Fig. 3 for both $\mathbf{M}^{-1}\mathbf{K}$ and $\mathbf{M}^{-1}\mathbf{K^B}$ serving as electromechanical model. The groupings for the model $\mathbf{M}^{-1}\mathbf{K}$ are computed by using its aligned eigenvectors in Algorithm 1. When $\mathbf{M}^{-1}\mathbf{K}$ serves as the model, the quantities Ncut_M and ϕ_M are still evaluated by using a symmetrized version of $\mathbf{K}$ that is obtained by averaging the elements above and below the main diagonal as $K_{ij}^S = (K_{ij} + K_{ji})/2$. For power networks without phase shifters, $K_{ij}^S = K_{ij}^B$, which means that the matrix $\mathbf{K^B}$ is used to evaluate (3) and (4) in all cases. The maximum number of machine groups is set to 14, which is a rather high number for a 48-machine system that is chosen to provide a general and broad comparison.

Algorithm 2: Improved Inertial Generator Aggregation.

Input: Power system model, coherent groups $\mathcal{C}_1, \ldots, \mathcal{C}_k$.

```
for l = 1 to k do
    x̂'_{d,eq} ← 20(Σ_{i∈C_l} 1/x'_{d,i})^{-1}
    x ← Range of numbers from 10^{-6} to x̂'_{d,eq}.
    for i = 1 to |x| do
        Aggregate group C_l with the basic method [18].
        x'_{d,eq} ← x[i]
        Compute the slow modes and store errors (9).
    end for
    Choose x'_{d,eq} for C_l as x[i] yielding smallest error (9).
end for
```

Output: Reduced power system model

The upper Figs. 3a and 3b show that the grouping algorithm from Section IV (shown in two variants: with and without the greedy refinement stage) performs equally or better than the classic grouping algorithm (the dash-dot green curve) in all test cases. All tested grouping algorithms have a peak in their eigenvalue error curves at $k = 4$, which also corresponds to the maximum of alignment cost in Fig. 2. This high alignment cost value implies that the four slowest electromechanical eigenvectors provide a limited amount of information to minimize the Ncut_M criterion. Therefore, the Ncut refinement algorithm in Section IV-C becomes more valuable to find lower Ncut_M values using the initial information contained in the eigenvectors. For $k = 4$, the complete Ncut minimization approach of Sections IV-A–IV-C (the solid black curve) is able to noticeably improve the machine grouping in terms of metric (9).

The lower Figs. 3c and 3d confirm the claim that minimizing the Ncut_M criterion is a good strategy to obtain accurate machine groupings based on slow coherency. As normalized cuts are normally increasing in value with the growing number of groups, we choose to show the ratios of the results by other algorithms to the result of our combined algorithm in Sections IV-A–IV-C (denoted by the $\dagger$ superscript), which allows us to represent the results for different group numbers on a similar scale. Thus, the results of our complete algorithm in Section IV are shown by the black horizontal line at the unity level, while the results of our proposed algorithm excluding Ncut refinement are shown by cyan bars, and the results of the classic slow coherency algorithm are shown by green bars. By comparing the results in Figs. 3a and 3b with their counterparts in Figs. 3c and 3d, it can be recognized that lower Ncut$M$ values are linked to lower slow modes approximation errors. Moreover, the complete algorithm in Section IV tends to produce both the lowest Ncut_M values and the lowest eigenvalue errors.

VI. Nonlinear Model Reduction Results

A. Improved Inertial Generator Aggregation Algorithm

The goal of nonlinear model reduction is to produce a reduced power system model consisting of standard power system elements (e.g., generators, loads, transformers) that is compatible with common time-domain simulation programs. This goal can

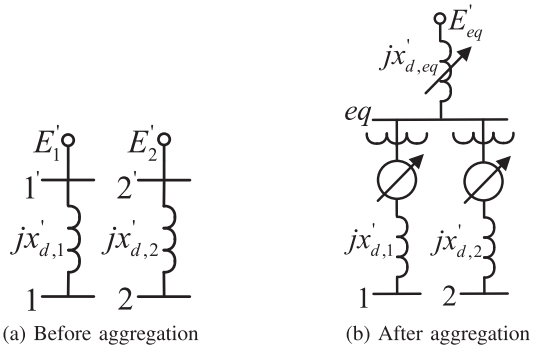

(a) Before aggregation (b) After aggregation

Fig. 4. Improved inertial generator aggregation algorithm.

be reached by replacing each coherent generator group by a single equivalent generator – this process is known as *generator aggregation* [30].

In [18], the inertial generator aggregation algorithm was proposed to alleviate the *stiffening effect* of the widely used Podmore generator aggregation algorithm. The stiffening effect manifests itself in the increased electromechanical mode frequencies of the reduced model compared to the original one. To reduce this effect, it was proposed to aggregate the coherent generators at their internal nodes instead of the terminal bus aggregation as in the Podmore method. Merging together the internal generator nodes of each coherent group as shown in [18] and linearizing the resulting reduced system produces the same model as the linear inertial aggregate model from Section V. From Fig. 3 it can be seen that the stiffening effect remains quite significant. For higher group numbers, the averaged metric in (9) decreases, but the error in the slow inter-area modes may increase.

As the persisting stiffening effect of the inertial aggregation algorithm may often lead to unsatisfactory nonlinear reduced models, a simple yet effective improvement is proposed. In Fig. 4, the initial and final stages of the inertial aggregation algorithm are illustrated for two generators represented by their classical models. Going from Fig. 4a to Fig. 4b involves aggregation of nodes $1'$ and $2'$ into node eq using the Zhukov bus aggregation method [31]. This includes adding ideal transformers and phase shifters in series with reactances $x'_{d,1}$ and $x'_{d,2}$ to preserve the initial power flow. The dynamic parameters of the equivalent generator are derived from the sum of swing equations of generators belonging to a coherent group $\mathcal{C}$ by assuming their incremental speeds and rotor angles to be the same (the coherency condition):

$$H_{eq} = \sum_{i \in \mathcal{C}} H_i, D_{eq} = \sum_{i \in \mathcal{C}} D_i \tag{10}$$

Where H_{eq} is the equivalent inertia constant, and D_{eq} is the equivalent damping constant.

In the original inertial aggregation algorithm, the effective reactance behind bus eq is zero (i.e., $x'_{d,eq} = 0$), which strictly corresponds to the aggregation of generator internal buses. However, we have noticed that it is possible to decrease the electromechanical frequencies of the reduced model by increasing the reactance $x'_{d,eq}$ from a value close to zero to some meaningful upper limit $\widehat{x}'_{d,eq}$. The improved inertial aggregation algorithm is summarized as Algorithm 2. In Algorithm 2, $\widehat{x}'_{d,eq}$ is set to 20 times $x'_{d,eq}$ of the Podmore algorithm, which is chosen empirically for studies on the NPCC 48-machine test system.

TABLE I
6-AREA GROUPINGS IDENTIFIED BY TWO METHODS

Area	Method	Machine numbers
1	Classic	1, 2, 3, 4, 5, 6, 7, 8, 9, 10
	Our	1, 2, 3, 4, 5, 6, 7, 8, 9, 10, 27, 28, 29, 30
2	Classic	11, 12, 13, 14, 15, 16, 17, 18, 19, 20, 21, 22, 23, 26, 31, 33, 34, 35, 36
	Our	11, 12, 13, 14, 15, 16, 17, 18, 19, 20, 21, 22, 23, 24, 25, 26, 31, 33, 34, 35, 36
3	Classic	24, 25, 27, 28, 29, 30, 43, 44, 45, 46, 47
	Our	43, 44, 45, 46, 47
4	Classic	32, 37, 38, 40, 41
	Our	32, 37, 38, 40, 41, 42
5	Classic	39, 42
	Our	39
6	Classic	48
	Our	48

Algorithm 2 preserves the advantages of the baseline approach [18] such as conceptual simplicity and possibility to independently aggregate each generator group. As shown in Section VI-B, Algorithm 2 is significantly more accurate, thus trading execution speed for accuracy. However, if execution speed is highly important, Algorithm 2 allows for massive parallelization. Clearly, both basic inertial aggregation and Algorithm 2 are only valid for generators represented by the classical model. However, representing external remote generators by the simplified 2^{nd} order model is well-accepted and often used in practice (e.g., in the DYNRED software [12] and in the Dutch transmission network model).

B. Six Area Grouping of NPCC 48-Machine Test System

As discussed in Section V-B, it is known that the NPCC 48-machine test system can be well decomposed into 9 areas based on its 9 slowest electromechanical modes. Our previous case study in Section V-B comes to the same conclusion, but it additionally identifies alternative area structures consisting of 3 and 6 areas (see Fig. 2). The present case study illustrates the validity of decomposing the NPCC system into 6 areas by using our grouping algorithm in Section IV. Additionally, the proposed improved inertial generator aggregation is shown to yield favorable results with our 6-area grouping that is given in Table I. The geographic locations of the machines in Table I can be found in multiple sources containing case studies based on the NPCC 48-machine test system (e.g., [3], [18]).

To be consistent with several previous studies (e.g., [18]), the simulated disturbance is a six-cycle short-circuit fault at Medway, which is cleared by opening the line from Medway to Sherman Road. The rotor angle swings following this disturbance are shown in Fig. 5 on per-coherent area basis. As Areas 5 and 6 each contain a single machine, only the transients in the four multi-machine areas are shown, with the individual

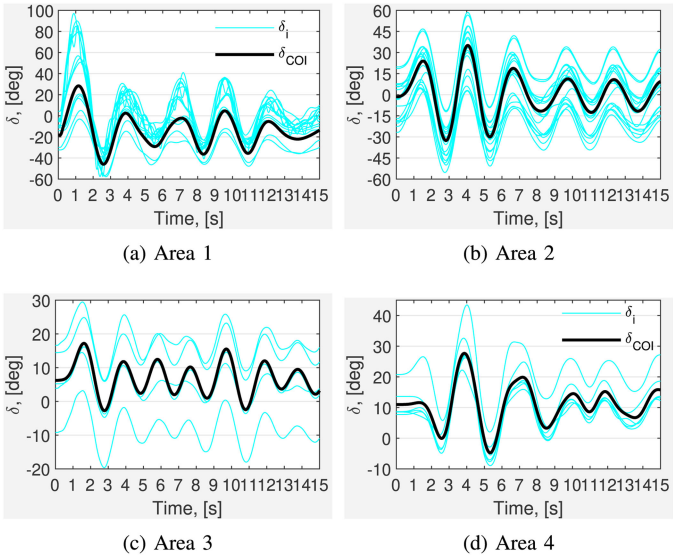

(a) Area 1 (b) Area 2

(c) Area 3 (d) Area 4

Fig. 5. Coherent swings in Areas 1–4 by our grouping method.

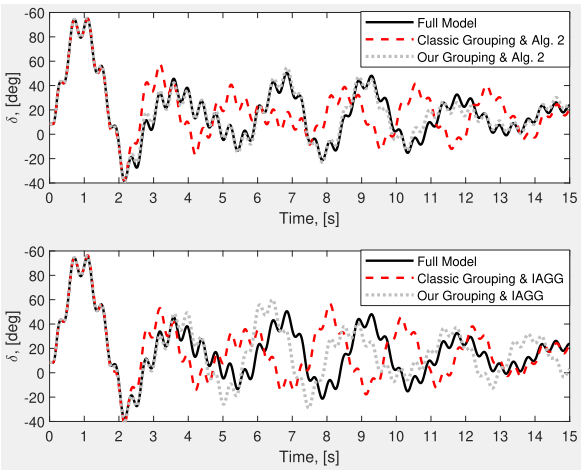

Fig. 6. Response of machine 4 for the Medway disturbance.

rotor angles plotted in cyan and the area center-of-inertia (COI) rotor angle plotted in black. In Fig. 5, the machines in each area swing coherently following the disturbance, which confirms the validity of the 6-area grouping.

Next, the suitability of the discovered 6-area grouping for nonlinear model reduction is examined. To further highlight the importance of coherency grouping accuracy, we perform one more nonlinear model reduction experiment involving the six areas returned by the classic slow coherency algorithm. As in [18], the unreduced study area is assumed to contain machines 1–10 for the both groupings, which corresponds to Area 1 (see Table I). The nonlinear model reduction results in the form of the rotor angle response of machine 4 to the Medway disturbance are shown in Fig. 6. In Fig. 6, the upper plot shows the outcomes of Algorithm 2, while the lower plot shows the outcomes of the original inertial aggregation method; the red graphs are based on the areas obtained with our grouping algorithm, while the

TABLE II
3-AREA GROUPING IDENTIFIED BY TWO METHODS

Area	Machine numbers
1	1, 2, 3, 4, 5, 6, 7, 8, 9, 10, 11, 12, 13, 14, 15, 16, 17, 18, 19, 20, 21, 22, 23, 24, 25, 26, 27, 28, 29, 30, 31, 33, 34, 35, 36
2	32, 37, 38, 39, 40, 41, 42
3	43, 44, 45, 46, 47, 48

green graphs are based on the areas returned by the classic grouping algorithm, and the blue graphs show the response of the unreduced system. The results in Figs. 5–6 confirm that the proposed grouping and aggregation framework is able to reliably identify slow coherent areas in a power system and to produce accurate reduced-order models from these areas. Noteworthy, the high frequency components in the rotor angle response in Fig. 6 arise due to the local mode oscillations between machines 4 and 5 that both share the same high-voltage bus without being aggregated, as they both belong to the unreduced Area 1.

C. Three Area Grouping of NPCC 48-Machine Test System

In Fig. 2, the lowest alignment cost values correspond to $k = 3$, and they are quite close to the lowest value of J equal to one (i.e., perfectly decoupled groups with negligible external connections). The low value of J is indicative of a distinct clustering of the rows of $\mathbf{Z}$ into the k mutually orthogonal groups. Therefore, the same three area grouping could be easily recovered both by the classic and new method (see Table II). By comparing Table II with the machine locations in [3], [18], it can be noticed that Area 2 in the West and Area 3 in the South are clearly geographically separated from the large Area 1 in the Northeast. Only machine 47 looks as an exception, as it is geographically (but not electrically) closer to Area 1.

Although the three area grouping reveals some valuable information about the system, it is likely to be too coarse for the most of practical purposes. For example, Area 1 is visibly too large and spans the most of the system. Moreover, it is no longer possible to take machine 48 as the angle reference in the reduced system model, as machine 48 is no longer a separate area, but a part of Area 3. Thus, closely reproducing the benchmark rotor angle time response [18] of the reduced system model for the Medway disturbance does not seem possible. However, we can point out that the rotor angle swings in Area 1 are similar to Fig. 5a, swings in Area 2 are very similar to Fig. 5b, and swings in Area 3 are very similar to Fig. 5c. These conclusions come as no surprise after comparing Tables I and II.

D. Sixteen Area Grouping of NPCC 48-Machine Test System

The goal of this concluding case study is to demonstrate the performance of the proposed machine grouping and aggregation techniques when the selected number of groups is relatively high. In particular, it may be more convenient for dynamic model reduction to operate on many small and compact generator groups as opposed to aggregating a few large areas. Thus, we have selected $k = 16$, which is close to $k = 17$ returned by

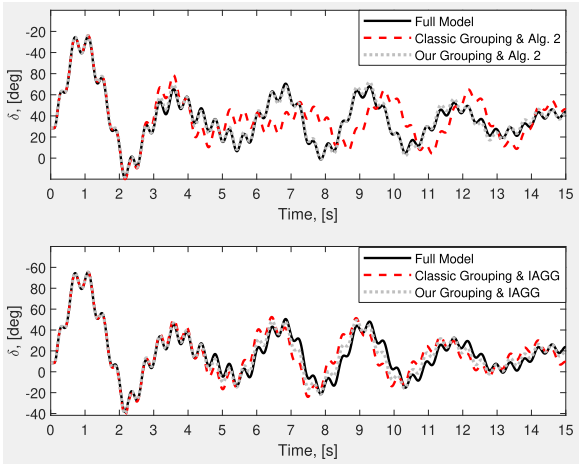

Fig. 7. Response of machine 4 (16-area groping).

the tight coherency algorithm in [18]. Selecting $k = 16$ also corresponds to the low alignment cost value of 1.11 if the $\mathbf{M}^{-1}\mathbf{K}$ model is used. The machine groups $\mathcal{C}_1, \ldots, \mathcal{C}_{16}$ returned by our algorithm are listed below:

$$\begin{aligned}
&\mathcal{C}_1 = \{1, 2\}, \mathcal{C}_2 = \{3, 4, 5\}, \mathcal{C}_3 = \{6, 7\}, \mathcal{C}_4 = \{8\},\\
&\mathcal{C}_5 = \{9, 10, 13, 14, 15, 23, 24, 25, 26\}, \mathcal{C}_6 = \{11, 12\},\\
&\mathcal{C}_7 = \{16, 17, 18, 19, 20, 21, 22\}, \mathcal{C}_8 = \{27, 28, 29, 30\},\\
&\mathcal{C}_9 = \{31, 33\}, \mathcal{C}_{10} = \{32, 37, 38, 40, 42\}, \mathcal{C}_{11} = \{34, 35\},\\
&\mathcal{C}_{12} = \{36\}, \mathcal{C}_{13} = \{39\}, \mathcal{C}_{14} = \{41\}, \mathcal{C}_{15} = \{48\},\\
&\mathcal{C}_{16} = \{43, 44, 45, 46, 47\}
\end{aligned} \tag{11}$$

where $\mathcal{C}_1, \ldots, \mathcal{C}_5$ constitute the unreduced study area.

The rotor angle time response of machine 4 has been simulated as described in Section VI-B, and the results are shown in Fig. 7. By comparing the lower plots of Figs. 6 and 7, it can be concluded that increasing the number of areas has a positive effect on the conventional grouping and aggregation techniques. This conclusion agrees with the decreasing eigenvalue approximation errors as k grows in Fig. 3. By comparing the upper plots of the two figures, it can be seen that the proposed grouping and reduction techniques also benefit from increasing k: the reduced model response nearly overlaps with the original one for $k = 16$. Finally, the 16 areas in (11) are significantly different both from the 16 areas by the classic grouping algorithm and the 17 areas by the tight coherency method.

VII. Conclusion

This paper has proposed a new accurate approach for identifying slow coherent generator groups in power networks. The presented connection between slow coherency and normalized cuts motivates the normalization of slow electromechanical eigenvectors by machine inertias to better reveal the orthogonal structure inherent in the slow coherency grouping problem. Furthermore, the robust spectral embedding alignment algorithm from our previous work was adjusted to robustly align mass-normalized electromechanical eigenvectors with the canonical coordinate system.

The aligned mass-normalized eigenvectors $\mathbf{Z}^*$ can be used to both meaningfully guide the selection of the number of groups and to produce the actual grouping by minimizing the Ncut_M criterion. To minimize Ncut_M more effectively, a new machine grouping algorithm specific to the problem in (3) was developed. This algorithm was shown to consistently outperform the other comparable methods. Moreover, the produced Ncut_M minimization results could not be further improved by the exact mixed-binary Ncut minimization program [21] after solving each case with Gurobi [32] for 30 minutes. Finally, an enhanced inertial aggregation algorithm was introduced to demonstrate the excellent suitability of our slow coherency grouping technique for producing nonlinear power system dynamic equivalents.

Although this paper was more focused on dynamic model reduction, we strongly believe that the proposed slow coherency grouping technique can be useful to other applications requiring coherent power system areas. Our usage of the basic $\mathbf{M}^{-1}\mathbf{K}$ model is less limiting than it may seem, as networks with voltage source inverter (VSI) generators can often be represented by a similar dynamic model (e.g., see [33]).

Acknowledgment

The authors would like to thank NWO and the consortium in the frame of this project, and highly appreciate fruitful discussions among all consortium partners related to this research.

References

[1] R. Podmore, "Identification of coherent generators for dynamic equivalents," *IEEE Trans. Power App. Syst.*, vol. PAS-97, no. 4, pp. 1344–1354, Jul. 1978.
[2] P. V. Kokotovic, B. Avramovic, J. H. Chow, and J. R. Winkelman, "Coherency based decomposition and aggregation," *Automatica*, vol. 18, no. 1, pp. 47–56, 1982.
[3] J. H. Chow, Ed., *Power System Coherency and Model Reduction*. New York, NY, USA: Springer-Verlag, 2013.
[4] L. Ding, F. M. Gonzalez-Longatt, P. Wall, and V. Terzija, "Two-step spectral clustering controlled islanding algorithm," *IEEE Trans. Power Syst.*, vol. 28, no. 1, pp. 75–84, Feb. 2013.
[5] J. Quirós-Tortós, R. Sánchez-García, J. Brodzki, J. Bialek, and V. Terzija, "Constrained spectral clustering-based methodology for intentional controlled islanding of large-scale power systems," *IET Gener. Transmiss. Distrib.*, vol. 9, no. 1, pp. 31–42, 2015.
[6] I. Tyuryukanov, J. Quirós-Tortós, M. Naglic, M. Popov, M. van der Meijden, and V. Terzija, "Controlled islanding of power networks based on graph reduction and spectral clustering," in *Proc. MedPower*, Belgrade, Serbia, 2016, pp. 1–6.
[7] I. Kamwa, A. K. Pradhan, G. Joos, and S. Samantaray, "Fuzzy partitioning of a real power system for dynamic vulnerability assessment," *IEEE Trans. Power Syst.*, vol. 24, no. 3, pp. 1356–1365, Aug. 2009.
[8] N. Xue and A. Chakrabortty, "Control inversion: A clustering-based method for distributed wide-area control of power systems," *IEEE Control Netw. Syst*, vol. 6, no. 3, pp. 937–949, Sep. 2019.
[9] V. Terzija *et al.*, "Wide-area monitoring, protection, and control of future electric power networks," *Proc. IEEE*, vol. 99, no. 1, pp. 80–93, Jan. 2011.
[10] M. Naglic, M. Popov, M. van der Meijden, and V. Terzija, "Synchronized measurement technology supported online generator slow coherency identification and adaptive tracking," *IEEE Trans. Smart Grid*, vol. 11, no. 4, pp. 3405–3417, Jul. 2020.
[11] N. Senroy, "Generator coherency using the Hilbert–Huang transform," *IEEE Trans. Power Syst.*, vol. 23, no. 4, pp. 1701–1708, Nov. 2008.

[12] F. Ma and V. Vittal, "Right-sized power system dynamic equivalents for power system operation," *IEEE Trans. Power Syst.*, vol. 26, no. 4, pp. 1998–2005, Nov. 2011.
[13] J. B. Ward, "Equivalent circuits for power flow studies," *AIEE Trans. Power Appl. Syst.*, vol. 68, no. 1, pp. 373–382, 1949.
[14] C. Sturk, L. Vanfretti, Y. Chompoobutrgool, and H. Sandberg, "Coherency-independent structured model reduction of power systems," *IEEE Trans. Power Syst.*, vol. 29, no. 5, pp. 2418–2426, Sep. 2014.
[15] G. Scarciotti, "Low computational complexity model reduction of power systems with preservation of physical characteristics," *IEEE Trans. Power Syst.*, vol. 32, no. 1, pp. 743–752, Jan. 2017.
[16] D. Romeres, F. Dörfler, and F. Bullo, "Novel results on slow coherency in consensus and power networks," in *Proc. Eur. Control Conf.*, 2013, pp. 1–6.
[17] J. H. Chow, *Time-Scale Modeling of Dynamic Networks With Applications to Power Systems*, Lecture Notes in Control and Information Sciences, vol. 46. Berlin, Germany: Springer-Verlag, 1982.
[18] J. H. Chow, R. Galarza, P. Accari, and W. W. Price, "Inertial and slow coherency aggregation algorithms for power system dynamic model reduction," *IEEE Trans. Power Syst.*, vol. 10, no. 2, pp. 680–685, May 1995.
[19] J. Shi and J. Malik, "Normalized cuts and image segmentation," *IEEE Trans. Pattern Anal. Mach. Intell.*, vol. 22, no. 8, pp. 888–905, Aug. 2000.
[20] S. Yu and J. Shi, "Multiclass spectral clustering," in *Proc. 9th Int. Conf. Comput. Vision*, 2003, pp. 313–319.
[21] N. Fan and P. M. Pardalos, "Multi-way clustering and biclustering by the ratio cut and normalized cut in graphs," *J. Comb. Optim.*, vol. 23, no. 2, pp. 224–251, 2012.
[22] I. Tyuryukanov *et al.*, "Discovering clusters in power networks from orthogonal structure of spectral embedding," *IEEE Trans. Power Syst.*, vol. 33, no. 6, pp. 6441–6451, Nov. 2018.
[23] E. Cotilla-Sanchez, P. Hines, C. Barrows, S. Blumsack, and M. Patel, "Multi-attribute partitioning of power networks based on electrical distance," *IEEE Trans. Power Syst.*, vol. 28, no. 4, pp. 4979–4987, Nov. 2013.
[24] P. M. Anderson and A. A. Fouad, *Power System Control and Stability*, 2nd ed., IEEE Press Power Engineering Series. Piscataway, NJ, USA: IEEE Press, 2003.
[25] G. Rogers, *Power System Oscillations*. New York, NY, USA: Springer, 2000.
[26] R. J. Sanchez-Garcia *et al.*, "Hierarchical spectral clustering of power grids," *IEEE Trans. Power Syst.*, vol. 29, no. 5, pp. 2229–2237, Sep. 2014.
[27] L. Zelnik-Manor and P. Perona, "Self-tuning spectral clustering," in *Proc. Adv. Neural Inf. Process. Syst.*, 2004, pp. 1601–1608.
[28] I. Tyuryukanov, J. Quirós-Tortós, M. Naglič, M. Popov, M. van der Meijden, and V. Terzija, "A post-processing methodology for robust spectral embedded clustering of power networks," in *Proc. 17th IEEE Int. Conf. Smart Technol.*, 2017, pp. 1–5.
[29] J. H. Chow and K. W. Cheung, "A toolbox for power system dynamics and control engineering education and research," *IEEE Trans. Power Syst.*, vol. 7, no. 4, pp. 1559–1564, Nov. 1992.
[30] A. Chakrabortty, J. H. Chow, and A. Salazar, "A measurement-based framework for dynamic equivalencing of large power systems using wide-area phasor measurements," *IEEE Trans. Smart Grid*, vol. 2, no. 1, pp. 68–81, Mar. 2011.
[31] J. Machowski, J. W. Bialek, and J. Bumby, *Power System Dynamics: Stability and Control*, 2nd ed. Hoboken, NJ, USA: Wiley, 2011.
[32] Gurobi Optimization, LLC, "Gurobi optimizer reference manual," 2020. [Online]. Available: http://www.gurobi.com
[33] P. J. Hart, R. H. Lasseter, and T. M. Jahns, "Coherency identification and aggregation in grid-forming droop-controlled inverter networks," *IEEE Trans. Ind Appl.*, vol. 55, no. 3, pp. 2219–2231, May-Jun. 2019.

Ilya Tyuryukanov (Member, IEEE) received the B.S.E.E. degree (Hons.) from Moscow Power Engineering Institute (Technical University), Moscow, Russia, the M.Sc. degree (Hons.) from RWTH Aachen University, Aachen, Germany, and the Ph.D. degree from the Delft University of Technology, Delft, the Netherlands in 2010, 2014, and 2020 respectively. He is currently a Postdoctoral Researcher at the Delft University of Technology, Delft, the Netherlands.

His research interests include machine learning and optimization techniques applied to power systems, in particular, wide-area control and protection.

Marjan Popov (Senior Member, IEEE) received the DiplIng. in electrical power engineering from the University of Saints Cyril and Methodius, Skopje, the Republic of Macedonia, in 1993 and the Ph.D. degree in electrical power engineering from the Delft University of Technology, Delft, The Netherlands, in 2002. In 1997, he was an Academic Visitor working on modeling SF6 circuit breakers with the Arc Research Group, University of Liverpool, Liverpool, U.K., where he is currently a Chevening Alumnus.

His major fields of interest are future power systems, large-scale power system transients, intelligent protection for future power systems, and wide-area monitoring and protection. Prof. Popov is a member of CIGRE and actively participated in WG C4.502 and WG A2/C4.39. In 2010, he received the Hidde Nijland Prize for extraordinary research achievements. He is a recipient of the IEEE PES Prize Paper Award and IEEE Switchgear Committee Award for 2011 and an Associate Editor for Elseviers *International Journal of Electric Power and Energy Systems*. He is also the Director of the Power System Protection Centre, The Netherlands.

Mart A. M. M. van der Meijden (Senior Member, IEEE) received the M.Sc. degree (Hons.) in electrical engineering from the Eindhoven University of Technology, the Netherlands, in 1981.

He is Part-Time Full Professor with the Department of Electrical Sustainable Energy of the Faculty of Electrical Engineering, Mathematics and Computers Science, Delft University of Technology, since 2011. His chair and research focus is on Large Scale Sustainable Power Systems. Prof. van der Meijden has more than 35 years of working experience in the field of process automation and the transmission and the distribution of gas, district heating and electricity. He is leading research programs on intelligent electrical power grids, reliable and large scale integration of renewable (wind, solar) energy sources in the European electrical power systems and advanced grid concepts. Since 2003 he is working with TenneT TSO, Europe's first cross-border grid operator for electricity. He is Manager R&D/Innovation and was responsible for the development of the TenneT long-term vision on the electrical transmission system. Prof. van der Meijden is a member of IEEE, ENTSO-E/RDIC, ETIP SNET, and CIGRE, and he has joined and chaired different national and international expert groups.

Vladimir Terzija (Fellow, IEEE) received the Dipl-Ing., M.Sc., and Ph.D. degrees in electrical engineering from the University of Belgrade, Serbia, in 1988, 1993, and 1997, respectively.

He is the EPSRC Chair Professor in Power System Engineering with the School of Electrical and Electronic Engineering, The University of Manchester, U.K. His current research interests include smart grid applications, wide-area monitoring, protection, and control, switchgear and transient processes, and ICT, data analytics and digital signal processing applications in power systems.

Prof. Terzija is Editor in Chief of the *International Journal of Electrical Power and Energy Systems*, Alexander von Humboldt Fellow, as well as a DAAD and Taishan Scholar. He is the National Thousand Talents Distinguished Professor at Shandong University, China.